Applied Surface Science xxx (xxxx) xxxx

Contents lists available at ScienceDirect

Applied Surface Science

journal homepage: www.elsevier.com/locate/apsusc

Full Length Article

Interface structures of inclined ZnO thin film on (0 1 1)-MgO substrate with bulk-like optical properties

Xuebin Yuan[a,c], Hua Zhou[a,b,*], Hui-Qiong Wang[a,c,*], Xiao-Dan Wang[a], Wei Geng[a], Huahan Zhan[a], Kim Kisslinger[d], Lihua Zhang[d], Mingchun Xu[b], Quark Y. Chen[e,f], Junyong Kang[a]

[a] Fujian Provincial Key Laboratory of Semiconductors and Applications, Collaborative Innovation Center for Optoelectronic Semiconductors and Efficient Devices, Department of Physics, Xiamen University, Xiamen 361005, PR China
[b] School of Physics, Shandong University, Jinan 250100, PR China
[c] Xiamen University Malaysia, Sepang 43900, Selongor, Malaysia
[d] Center for Functional Nanomaterials, Brookhaven National Laboratory, Upton, NY 11973, USA
[e] Department of Physics and Center for Nanoscience and Nanotechnology, National Sun Yat-Sen University, Kaohsiung 80424, Taiwan
[f] Texas Center for Superconductivity and Department of Physics, University of Houston, Houston, TX 77204, USA

ARTICLE INFO

Keywords:
Inclined growth
Interface structure
ZnO film
MgO substrate
Optical property

ABSTRACT

Combining different phase structure materials with unique properties to design novel devices plays a significant role in the development of modern electronics. Here, we explore the characteristics of this type of complex interface and epitaxy structures based on the coupling between hexagonal ZnO film and cubic MgO substrate. The ZnO film was prepared by the molecular beam epitaxy technique on the MgO (0 1 1) substrate. The analysis results from the *in situ* reflection high energy electron diffraction patterns, X-ray diffraction (XRD)-pole figures and high resolution transmission electron microscopy images demonstrate that the film exhibits two-fold symmetry domains with a growth direction deviated from c-axis at about 31° along the [0 1 0] MgO or [0 $\bar{1}$ 0] MgO azimuth. Despite the intertwined diffusion from Zn and Mg atoms in the interface, which is the possible origin of a blue shift of about 0.083 eV in the Photoluminescence (PL) spectrum, the inclined film shows a full width at half maximum value that is close to the reported value from the high quality film. This work hopefully provides useful insights to the design and exploration of the novel optoelectronic devices that involve the integration of materials with different structure and different properties.

1. Introduction

Putting thin-film materials with unique properties of their own on a substrate of different crystal structures has become a common strategy in seeking novel device functions in modern electronics [1–4]. For example, optoelectronic semiconductor films such as ZnO [5–6] and GaN [7–10], or other 2-dimenional materials of hexagonal symmetry, such as graphene [11–14]and MoS_2[15], were frequently prepared on cubic substrates such as Si, GaAs, and MgO, etc. [16–19]. Uses of such heterostructures have indeed helped solved some problems confronting isomorphic material structures. It is well-known that, for example, GaN thin films grown on c-oriented substrate of α-Al_2O_3 usually lead to an internal electric field along the c-axis that would lead to reduced quantum efficiency in what is called quantum-confined Starks effect [20–21]. Nevertheless, this detrimental effect could be surmounted by use of (0 0 1)-oriented $LiAlO_2$ substrates of cubic symmetry, as having been demonstrated by Waltereit et al. [22] experimentally. Similar successes have also been achieved on $LiGaO_2$ and $LaAlO_3$ substrates [23–24].

Similar to GaN, ZnO is a popular optoelectronic semiconductor of stable hexagonal symmetry because of its wide band-gap (~3.4 eV) [25], large exciton bonding energy (~60 meV) [25] and large piezoelectric coefficients [25–26]. It has been made into heterostructures with other conventional semiconductors or transition metal oxides, among others, for optoelectronic and memory device applications. Cagin and Zhou et al., for example, had ZnO films of a variety of orientations placed on substrates of cubic symmetry, NaCl [27], $SrTiO_3$ [28], and MgO [29,30], while Bera et al. [31] have further obtained a new type of optical switches with faster response through ZnO nanowires or films on $SrTiO_3$ that exhibits unique electrical transport properties. However, similar to GaN films or 2D materials grown on cubic substrates, these ZnO films take on extremely complex growth

* Corresponding authors at: Fujian Provincial Key Laboratory of Semiconductors and Applications, Collaborative Innovation Center for Optoelectronic Semiconductors and Efficient Devices, Department of Physics, Xiamen University, Xiamen 361005, PR China.
E-mail addresses: zhouhua2018@sdu.edu.cn (H. Zhou), hqwang@xmu.edu.cn (H.-Q. Wang).

https://doi.org/10.1016/j.apsusc.2019.144781
Received 4 September 2019; Received in revised form 20 October 2019; Accepted 18 November 2019
Available online 27 November 2019
0169-4332/

paths as reflected in the often-unexpected orientations and the associated interfacial structures, particularly those tilted away from major crystallographic axes in some inclined growth direction [32,33]. As a consequence, precise controls of growth parameters to achieve good epitaxy for these films become necessary, albeit often also found a formidable pursuit.

Indeed, we have encountered such complexities on the subject matter of this report regarding the inclined growth of ZnO films on MgO substrates. Single crystals of MgO has been widely used as a substrate in many fields ranging from catalytic surfaces [34,35], magnetic thin films [36] and, among many others, exploratory novel devices [37]. We have in this work the ZnO thin films grown on (0 1 1)-oriented MgO substrates by molecular beam epitaxy (MBE), of which the details of instrumentation have been described elsewhere [30,38]. Briefly stated here, atomic force microscopy (AFM), high resolution transmission electron microscopy (HRTEM), X-ray diffraction (XRD), and *in situ* reflection high energy electron diffraction (RHEED) were employed to characterize the inherent crystal structures regarding the inclined growth, while photoluminescence (PL) spectroscopy was carried out to study the relevant optical properties. This work aims to better understand how the ZnO films of wurtzite structure would engage with the MgO of rock-salt structure, especially on the specifics of involved inclination in regards to their epitaxial relations.

2. Experiment methods

The MgO (0 1 1) substrate was cleaned three times sequentially by acetone ethanol in the ultrasonic bath. Before growth, the substrate was annealed at about 500 °C for 60 min with a plasma power of 250 *w* and oxygen pressure of 5×10^{-5} mbar. Growth and Zn source temperature were 240 °C and 330 °C, respectively, and oxygen pressure was kept at 1×10^{-5} mbar with a plasma power of 180 W.

In-situ reflection high-energy electron diffraction (RHEED) was used to characterize the surface and interface structures and the film morphology was further examined by atomic force microscopy (AFM). The interface relationship was characterized by X-ray Diffraction - pole figure and phi-scan, while the interface atomic structure was probed by a JEM-200CF high resolution transmission electron microscope with a FIB system used to prepare the samples. Photoluminescence (PL) was performed to determine the optical properties.

3. Results and discussions

Atomically flat surface of (0 1 1) MgO substrates were first obtained by annealing for one hour at about 550 °C before growth. Fig. 1(a) and (b) show their corresponding RHEED diffraction patterns after annealing captured along the $[0\ 1\ \bar{1}]_{MgO}$ and $[1\ 0\ 0]_{MgO}$ orthogonal axes, respectively. The bright Kikuchi lines (as indicated by the red arrows) in these two patterns suggest that the MgO substrate surfaces are indeed measurably flat at atomic scales after annealing. As the film growth began, these lines diminished and the streaks evolved into spotty patterns, as seen in Fig. 1(c) and (d) viewed along the $[1\ \bar{2}\ 1\ 0]_{ZnO}$ and $(1\ 0\ \bar{1}\ 1)^*_{ZnO}$ directions respectively. Here, the $(10\bar{1}1)^*_{ZnO}$ represents the normal of the ZnO (1 0 $\bar{1}$ 1) plane. The ZnO-film growth is thus believed to have proceeded in island mode, as is corroborated by the AFM images of grainy surface morphology shown in Fig. 1(f).

Existing in the RHEED patterns of the $[0\ \bar{1}\ 1]_{MgO}$ zone, i.e., for those with the probing electron beam incident along the $[0\ \bar{1}\ 1]_{MgO}$ direction, are two sets of diffraction spots, as distinguished by the blue and red circles, representative of a {1 0 $\bar{1}$ 3}-oriented ZnO crystals of Wurtzite symmetry, albeit slightly tilted off the substrate surface by rotating around [$\bar{1}$ 2 $\bar{1}$ 0], namely, one of the three $\hat{a}$-axes, by about $\pm$ 1. 66°, resulting in distinct mildly-twinned structural domains in the film. This is so concluded from the angle of largely 60° subtended between the two $\hat{c}$-axes contrasted with blue and red colors in the RHEED pattern of Fig. 1(c), instead of the $31.66^\circ \times 2 = 63.32^\circ$ expected between two {1 0 $\bar{1}$ 3} planes rotated 180° around the $\hat{c}$-axis. Each set of the patterns is characteristic of a ZnO [1 $\bar{2}$ 1 0]-zone diffraction pattern of a {1 0 $\bar{1}$ 3}-oriented ZnO crystal, for which [0 0 0 1] and [1 0 $\bar{1}$ 0] make up two major orthogonal basis vectors. Evaluated in the reciprocal space based on the diffraction peaks, therefore, as illustrated by the two perpendicular red (or blue) arrows, the basis vectors is corresponding to $(\vec{c})^*$ and $\left(\frac{\sqrt{3}}{2}\vec{a}\right)^*$, respectively. The ratio of the distances of adjacent spots in the perpendicular directions is calculated to be about 0.58, largely falling within acceptable tolerance in the range comparable to the ideal value of $\frac{\frac{\sqrt{3}}{2}a}{c}$ 0.54, consistent with what is expected of the {1 $\bar{2}$ 1 0} family of planes of ZnO single crystals. In Fig. 1(e), an atomic model is provided for reference. With $[0\ 1\ \bar{1}]_{MgO}$ and $[1\ \bar{2}\ 1\ 0]_{ZnO}$ now established as the zone axes of observation, it can hence be concluded with $[0\ 1\ \bar{1}]_{MgO}//[1\ \bar{2}\ 1\ 0]_{ZnO}$ as one of the two necessary epitaxial relations. This being said, the angle between the two $(\vec{c})^*$ vectors in blue and red is indeed measured to be about 60°, as mentioned above, while ideal geometric angle is 63.32° between the (1 0 $\bar{1}$ 3) and ($\bar{1}$ 0 1 3)-planes, and, as to be further discussed below based on the X-ray pole figure data, the lack of a six-fold symmetry readily hints at an inclined $(1\ 0\ \bar{1}\ 3)_{ZnO}$ with respect to $(0\ 1\ 1)_{MgO}$.

To further determine the epitaxial relations, X-ray scans of the (0 0 0 2) and (1 0 $\bar{1}$ 0) pole figures of the ZnO film were performed, and the results are given in Fig. 2(a) and (b), respectively. The (0 0 0 2) pole figure shows two diffraction spots 180° to each other at 31° of χ-angle, as indicated by the red arrows in Fig. 2(a). The absence of six-fold symmetry reflects the fact of a misorientation of some kind, but then the two-fold symmetry observed instead of a one-fold symmetry expected of a tilted $(1\ 0\ \bar{1}\ 3)_{ZnO}$ plane for its Wurtzite structure probed along $[1\ \bar{2}\ 1\ 0]_{ZnO}$ hints at the presence of twinning between tilted (1 0 $\bar{1}$ 3)- and ($\bar{1}$ 0 1 3)-planes in coexistence and supports the twinned RHEED patterns observed in the same $\hat{a}$-zone as analyzed earlier in regard to a $\pm$ 1. 66° tilting towards each other between the two $\hat{c}$-axes of two domains which should have subtended an angle of $31.66^\circ \times 2 = 63.32^\circ$, but actually was measured to be 60°. This discrepancy of 3. 32° is understood as an outcome of rotating the $\hat{c}$-axis of each domain by $3.32^\circ \times \frac{1}{2} = 1.66^\circ$ around the $\hat{a}$-axis of ZnO which is parallel to the intersecting line between (1 0 $\bar{1}$ 3)- and ($\bar{1}$ 0 1 3)-planes.

The (1 0 $\bar{1}$ 0)-pole figure shows six diffraction spots at $(\chi, \varphi) = (59^\circ, 0^\circ), (74^\circ, 63.5^\circ), (74^\circ, 116.5^\circ), (59^\circ, 180^\circ), (74^\circ, 243.5^\circ),$, and $(74^\circ, 296.5^\circ)$ as shown and indicated by the arrows in Fig. 2(b) with the first φ–angle referenced as $\varphi = 0^\circ$at $\chi = 59^\circ$. The first set has two peaks at $\chi \approx 59^\circ$ with φ-angles spaced 180° in between, while the second has a total of 4 peaks at $\chi = 74^\circ$. Close to this angular position $\chi = 59^\circ$, in spherical coordinates with χ as the polar angle and φ the azimuthal, lies a peak of the $\hat{m}$-pole that represents the diffraction from the $\hat{m}$-planes of the (1 0 $\bar{1}$ 3) or ($\bar{1}$ 0 1 3)-planes of ZnO with the $\hat{\chi}$-axis of the goniometer parallel to the $\hat{a}$-axis of ZnO and, ideally, $\hat{m}_{ZnO} \wedge [1\ 0\ \bar{1}\ 3]_{ZnO} = 57.84^\circ$. The small discrepancy of 1. 16° between the measured 59° and the ideal value of 57. 84° is considered as related to the $\pm$ 1. 66° tilting articulated in discussing the RHEED data in Fig. 1(a).

With the geometric relation largely in place, one needs to verify the consistency of the φ-angles of the $\hat{m}_{ZnO}$-pole figure in sequence of 0°, 63. 5°, 116. 5°, 180°, 243. 5° and 296. 5°. What follows is to first make sense of the spacing of $\pm$ 63. 5° neighboring the reference peak at (59°, 0°). Simple solid geometric analysis would show that in an ideal case the three neighboring peaks at (74. 56°, −63. 5°), (57. 84°, 0°), a nd (74. 56°, 63. 5°) in fact represent the three corresponding neighboring $\hat{m}$-plane diffraction peaks with the middle reference peak at (57. 84°, 0°) from the specific $\hat{m}$-plane whose $\hat{a}_{ZnO}$-axis is parallel to the χ–axis of the goniometer when the diffraction conditions are fulfilled. In other words, the reference peak arises from the $\hat{m}$-plane that has

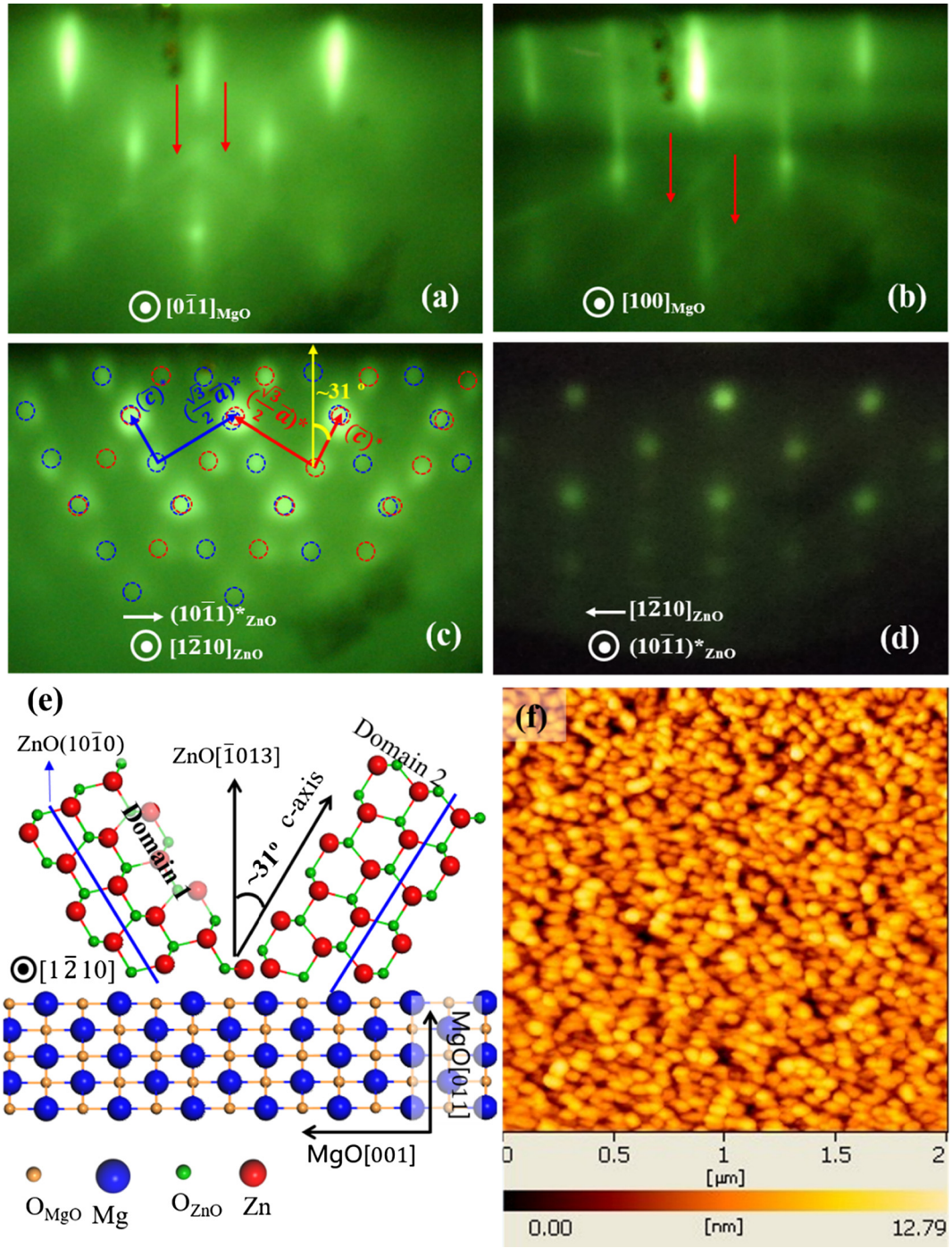

Fig. 1. (a) and (b) RHEED patterns from the MgO (0 1 1) substrate after annealing along the [100] and [0$\bar{1}$1] azimuth, respectively, displaying bright Kikuchi lines, as marked by the red arrows. (c) and (d) RHEED patterns from the grown ZnO film where yellow arrow represents the growth orientation and blue and red circle arrays indicate two sets of diffraction spots, respectively. (e) An atomic model from the side view along the ZnO[1 $\bar{2}$ 1 0] or MgO[0 $\bar{1}$ 1] direction, showing two kinds of different ZnO domains based on the results of the RHEED patterns. (f) AFM image from the ZnO film.

$\hat{a}_{ZnO}$, given as [$\bar{1}$ 2 $\bar{1}$ 0]$_{ZnO}$ for convenience as the convention in the following discussions, as the zone axis that makes up the plane of incidence with the probing beam, whether electron or X-ray. The corresponding zone-axes of the two neighboring peaks, on the other hand, would then be [6 $\bar{3}$ $\bar{3}$ $\bar{1}$]$_{ZnO}$ and [$\bar{3}$ $\bar{3}$ 6 1]$_{ZnO}$ for the two peaks at (74. 56°, ±63. 5°). In simpler terms these three zone axes can be described as $\hat{a}_3 + \frac{1}{3}\hat{c}$, $\hat{a}_2$, and $\hat{a}_1 - \frac{1}{3}\hat{c}$. The small discrepancy of the –angle is simply a result of the small ± 1. 66° tilts around the $\hat{a}_2$-axis, viz. [$\bar{1}$ 2 $\bar{1}$ 0]$_{ZnO}$, of the (1 0 $\bar{1}$ 3)$_{ZnO}$ or ($\bar{1}$ 0 1 3)$_{ZnO}$ twinning planes. Indeed, one can readily show that [6 $\bar{3}$ $\bar{3}$ $\bar{1}$]$_{ZnO}$∧ [$\bar{3}$ $\bar{3}$ 6 1]$_{ZnO}$ ≈ 63. 83° × 2 = 127. 66°, as compared to what was measured by the $\hat{m}$-pole figure of 63. 5° × 2 = 127°. This difference of 0. 66° can easily be reconciled with the ± 1. 66° tilting of the [1 0 $\bar{1}$ 3]$_{ZnO}$ and [$\bar{1}$ 0 1 3]$_{ZnO}$ toward each other, as discussed earlier. With this understanding, the epitaxial relations can be concluded as (1). [1 $\bar{2}$ 1 0]$_{ZnO}$//[0 1 $\bar{1}$]$_{MgO}$ according to the indices of the RHEED patterns in Fig. 1(c) that concluded both as the zone-axes, and (2). With [1 $\bar{2}$ 1 0]$_{ZnO}$ as the rotating-axis, [1 0 $\bar{1}$ 3]$_{ZnO}$ ∧ [0 1 1]$_{MgO}$= [$\bar{1}$ 0 1 3]$_{ZnO}$ ∧ [0 1 1]$_{MgO}$= 1. 66° (Here, the symbol ˆ means an angle between two crystal array directions), the ZnO film grew into a tilt-

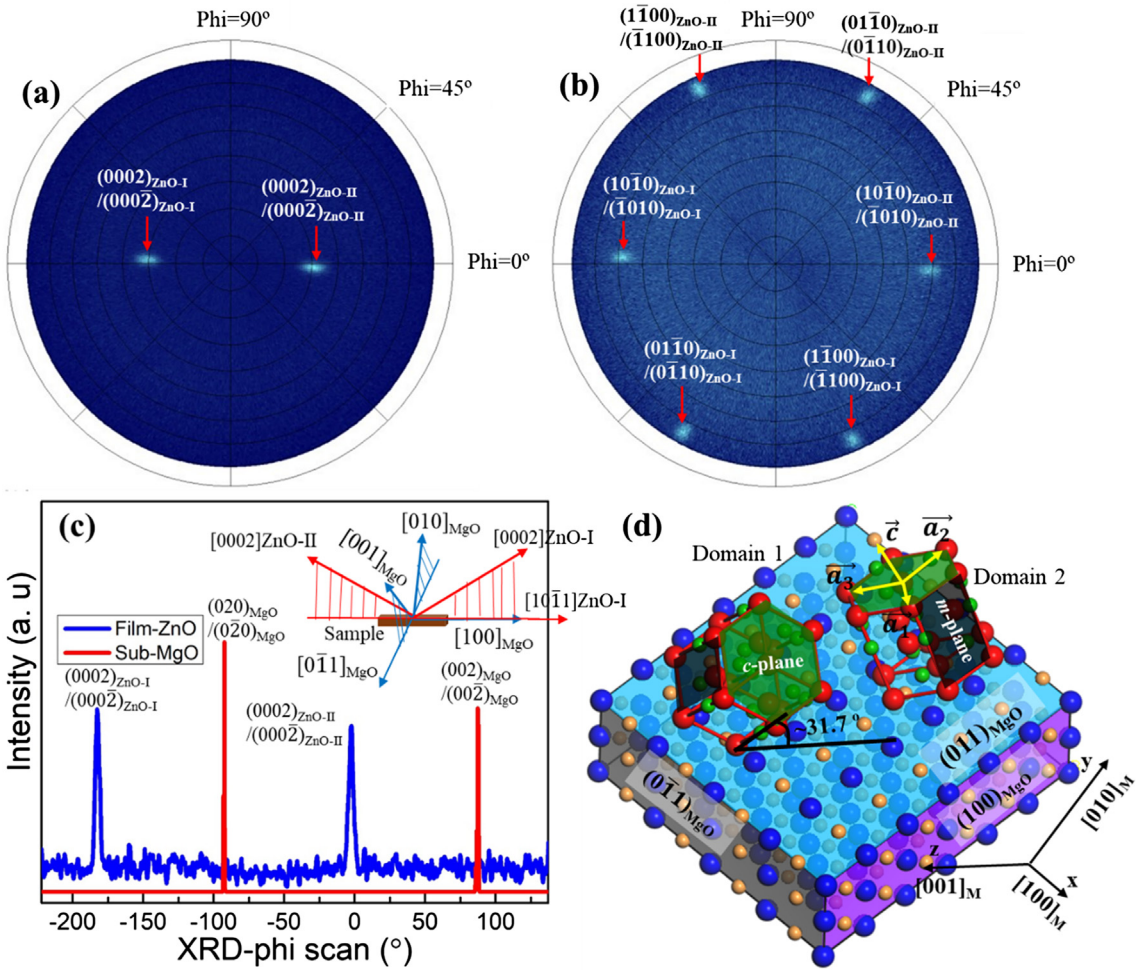

Fig. 2. (a) and (b) XRD pole figures from the {0 0 0 2} and {1 0 $\bar{1}$ 0} reflections of the incline film, respectively; (c) XRD phi-scan results from the {0 0 0 2} reflection of the incline ZnO film and {0 0 1} reflection of the (0 1 1) MgO substrate, where the inset displays a schematic of the phi-scan with crystalline directions. (d) Corresponding 3D atomic model, where black and green semi-transparent areas represent m- and c-planes of ZnO, respectively.

twins structure with a twin angle of 3. 32°. Hence, in essence, the ZnO sample is described as growing into a structure of ± 1. 66° tilt-twins off the substrate normal of $[0\ 1\ 1]_{MgO}$ in an otherwise would-be perfectly (1 0 $\bar{1}$ 3)-oriented epitaxial thin film on [0 1 1]-oriented MgO substrate.

Fig. 2(c) shows the corresponding phi-scan images from the (0 0 0 2)/(0 0 0 $\bar{2}$) plane of the ZnO film ((2θ, χ) = (34.4°, 31.3°)) and {0 0 1} plane of the MgO substrate ((2θ, χ) = (42.3°, 45°)). Fig. 2(d) displays the corresponding 3-dimensional atomic model accordingly, clearly illustrating these interface relationships and two types of domains with an incline of about 31° to [0 1 $\bar{1}$]MgO and [0 $\bar{1}$ 1]MgO azimuths, respectively. Here, semi-transparent green, black, light blue and gray areas represent c- and m-plane of ZnO film, surface and side planes of MgO substrate, respectively, and yellow arrows represent the basis vectors of ZnO.

To reveal the micro-structures of the interface and boundary for the incline growth, the ZnO film was further characterized by TEM, as shown in Fig. 3(a–g). Fig. 3(a) is the corresponding low-magnification TEM image on the zone axis of MgO [0 $\bar{1}$ 1], showing about 60 nm of film thickness. Here, red and green dashed lines represent the interface of ZnO/MgO and grain boundaries, respectively. Apparently, there display two types of parallel stripes at the adjacent regions, indicative of two kinds of domains in the film. Fig. 3(b) corresponds to selected area electron diffraction (SAED) image, also showing two sets of diffraction spots, as labelled by the red and yellow dots, respectively, consistent with the RHEED pattern captured at the MgO [0 $\bar{1}$ 1] azimuth (as shown in Fig. 1(c)). The bright spots are from the diffraction of substrate, as labelled by the light blue arrows. This SAED pattern reflects that the lattice between film and substrate follows a registry close to the relationship as bellow, with a few degrees of angle deviation:

[0 0 0 2][1 $\bar{2}$ 1 0]ZnO-| // [1 1 1][0 $\bar{1}$ 1]MgO;
[0 0 0 2][1 $\bar{2}$ 1 0]ZnO-‖// [1 1 1][0 $\bar{1}$ 1]MgO.

It is worth pointing out that the angles between [0 0 0 2] and (1 0 $\bar{1}$ 1)*$_{ZnO}$ (~61°) is close to the angle between [1 1 1]MgO and [1 0 0]MgO (~55°). This result also suggests (1 0 $\bar{1}$ 1)*$_{ZnO}$// $[1\ 0\ 0]_{MgO}$, consistent with the analysis of XRD pole figures.

Fig. 3(c) shows a high resolution TEM image, revealing that the c-axis of the two domain exhibits an incline of about 31° along the growth orientation, as illustrated by the yellow arrows. Yellow and red dashed curve lines show the grain boundary of Domains 1 and 2 and the ZnO/MgO interface, respectively. Because of the large mismatch and the phase structure difference between film and substrate, some defects appear at the interface, as illustrated by the red arrows in Fig. 3(c). Fig. 3(d) shows the high resolution image of ZnO film captured along [1 0 0] MgO azimuth. From the amplified image of the area at the interface as labelled by the red rectangle in image (d), one can see the hazy rhombus structure, as illustrated by the red solid dots in Fig. 3(e). In fact, the top view of the atomic model of ZnO (1 0 $\bar{1}$ 1) plane (as shown in Fig. S1 in Supporting Information) displays a perfect dot array

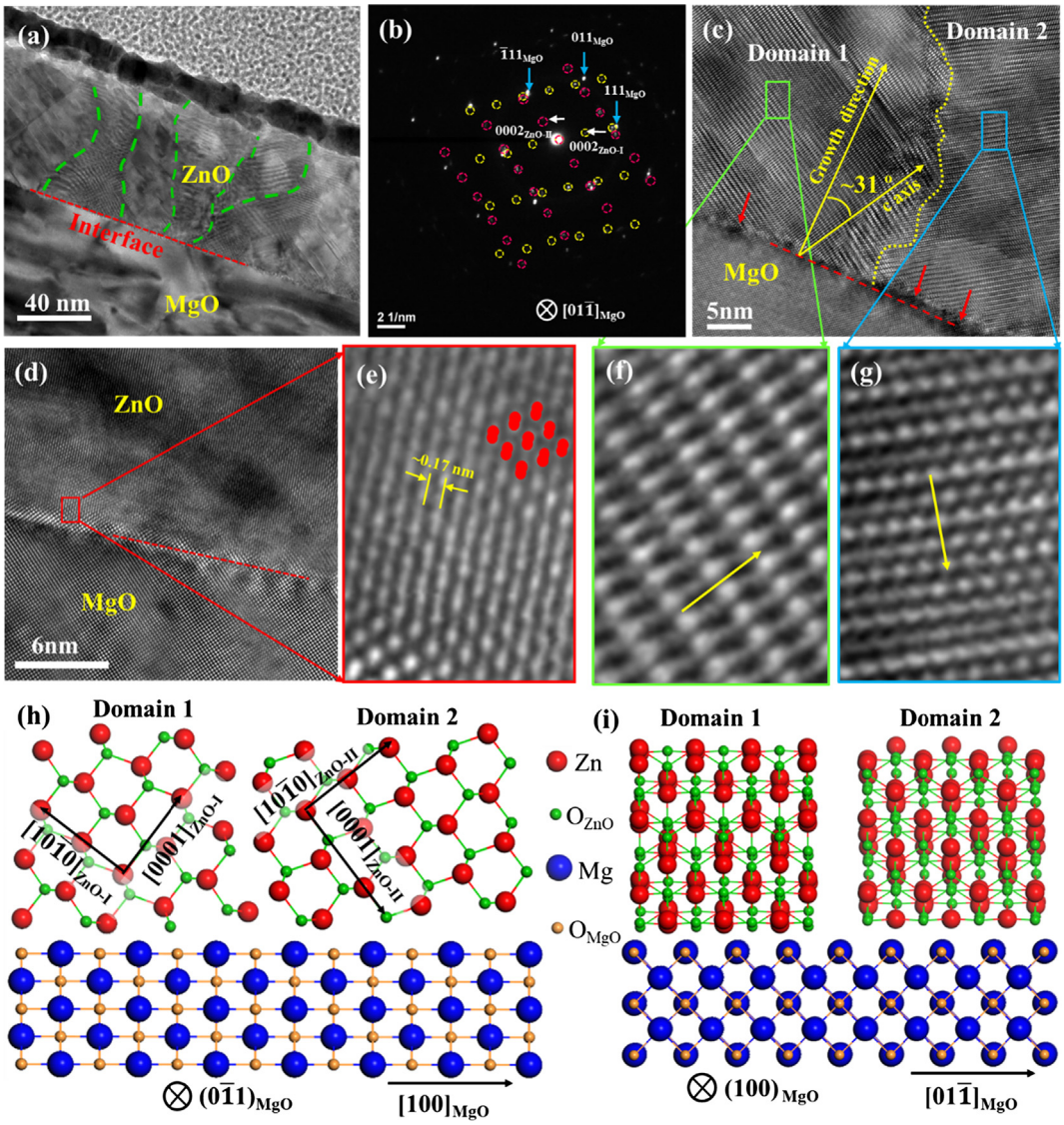

Fig. 3. (a) Cross-sectional low magnification TEM image captured along the zone-axis of [0 1 $\bar{1}$]MgO, where red straight line and green curve lines represent interface and grain boundary, respectively. (b) The corresponding SAEDP pattern, where red and yellow circle arrays represent two sets of diffraction spots. (c) The corresponding high-resolution TEM image, where yellow curve line shows the boundary between Domains 1 and 2. (d) The high-resolution TEM image on the zone-axis of [1 0 0]MgO. (e–g) The corresponding amplified images of the area as labelled by the red, green and blue rectangles in Figures (d) and (c). (h,i) The atomic models from the side views along [0 $\bar{1}$ 1]$_{MgO}$ and [1 0 0]$_{MgO}$ azimuths, respectively.

of rhombus geometry structure. Moreover, the distance between the adjacent planes is about 0.17 nm, close to $a_{ZnO}/2$. These results suggest that the high resolution TEM image in Fig. 3(d) presents the atomic array structures nearly along the film (1 0 $\bar{1}$ 1) plane, also indicating (1 0 $\bar{1}$ 1)*$_{ZnO}$//(1 0 0)$_{MgO}$. Here, (1 0 $\bar{1}$ 1)*$_{ZnO}$ represents the normal of the (1 0 $\bar{1}$ 1)$_{ZnO}$ plane. Fig. 3(f) and (g) are the corresponding amplified images of the areas as labelled by the green and blue rectangles in Fig. 3(c). In essence, the growth orientation of film on a substrate prefers the minimum energy and domain rotation number with lattice matching. The ZnO films grown on the (0 1 1)MgO substrate exhibit the orientation of [1 0 $\bar{1}$ 3] azimuth with two rotation domains with an angle of about 31° could probably serve the purpose. Fig. 3(h) and (i) show the atomic models of the side view from the [0 $\bar{1}$ 1]$_{MgO}$ and [1 0 0]$_{MgO}$ azimuth, respectively. It is worth noting that the atomic models of Domain 1 and 2 along the [1 0 0]$_{MgO}$ azimuth are very similar, indicating that the top view of the ZnO (1 0 $\bar{1}$ 1) plane after rotating 180° remains almost the same. It also means that the high resolution TEM images of Domains 1 and 2 on the zone the [1 0 0]$_{MgO}$ azimuth is almost identical, which explains why different domain regions are not observed in Fig. 3(d).

From the discussions of the results of RHEED patterns, XRD pole-figures and TEM images, we can obtain the interface relationships of the slightly tilted {1 0 $\bar{1}$ 3}-oriented ZnO films on the MgO (0 1 1) substrate:

± 1.66-tilited {$\bar{1}$ 0 1 3}(1 0 $\bar{1}$ 1)*[1 $\bar{2}$ 1 0]$_{ZnO-I}$//(0 1 1)[1 0 0] [0 $\bar{1}$ 1]$_{MgO}$;
± 1.66-tilited {1 0 $\bar{1}$ 3}(1 0 $\bar{1}$ $\bar{1}$)*[1 $\bar{2}$ 1 0]$_{ZnO-II}$//(0 1 1)[1 0 0] [0 $\bar{1}$ 1]$_{MgO}$.

Here, star represents the normal of the corresponding plane. In essence, this type of interface coupling with a tilted growth orientation well agrees with the simple concepts of coincidence lattices with negligible tolerance in the two orthogonal directions, as shown in Fig. S2 (as available in Supporting Information). Since a_{ZnO} = 3.249 Å, c_{ZnO} = 5.205 Å, a_{MgO} = 4.211 Å, it is simple to calculate the lattice lengths in their orthogonal directions as follows: $d_{[100]MgO}$ = 4.211 Å, $d_{[0\bar{1}1]MgO}$ = 2.978 Å, $d_{(10\bar{1}1)*ZnO}$ = 19.835 Å, $d_{(1\bar{2}10)*ZnO}$ = 3.249 Å.

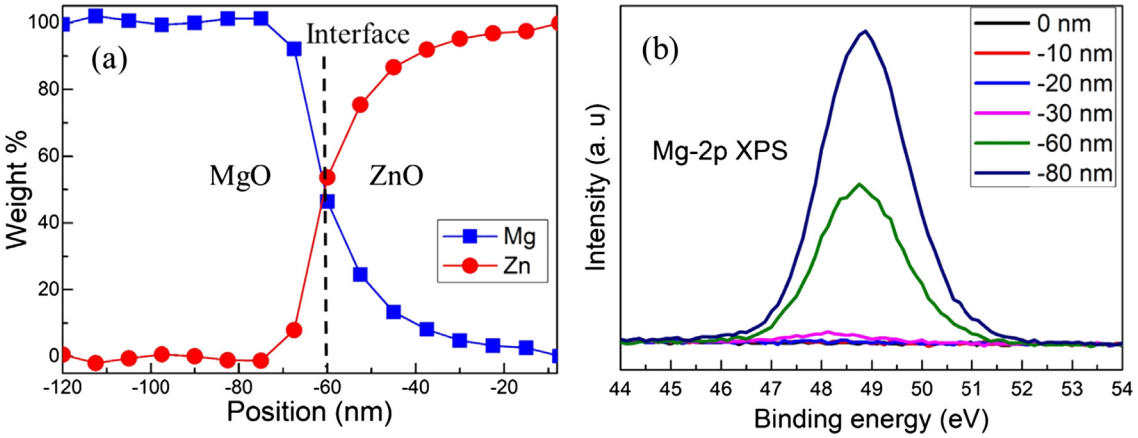

Fig. 4. (a) EDS results across the interface from the substrate to the film; (b) Mg-2p XPS spectra from the top surface of the film to the substrate across the interface.

Therefore, the MgO(0 1 1) substrate is able to match with the ZnO (1 0 $\bar{1}$ 3) oriented film as follows:

$3d_{(10\bar{1}1)*ZnO} = 14\ d_{[100]MgO}$ with a mismatch of about 0.9%;
$11d_{(1\bar{2}10)*ZnO} = 12d_{[0\bar{1}1]MgO}$ with a mismatch of about 0.01%.

That is to say, such domain matching has two rectangular MgO (0 1 1)-planes as a substrate unit cell, matching a $14d_{[100]MgO} \times 12d_{[0\bar{1}1]MgO}$ rectangle of 58.954 Å × 35.736 Å with a 59.505 Å × 35.739 Å array of $3d_{(10\bar{1}1)*ZnO} \times 11d_{(1\bar{2}10)*ZnO}$ rectangle, as illustrated in Fig. S2.

To the best of our knowledge, the adsorption energy of Mg atom in MgO crystal surface is small enough (~0.45 eV) [39], that it is inevitably to exhibit diffusion at the interface of ZnO/MgO. In fact, the ZnO film at the interface shows cubic phase structure, as demonstrated by Fig. S3 (as available in Supporting Information). This result implies that the film phase at the interface is an alloy structure of ZnMgO. In order to further verify this point, we characterize the evolution of the Mg and Zn contents from the substrate to the film surface by X-ray photoelectron spectroscope (XPS) and Energy Dispersive Spectrometer (EDS), as shown in Fig. 4(a) and (b), respectively. The EDS image (Fig. 4(a)) show the substrate area near the interface contains numerous Zn atoms, indicating negative diffusion at the interface during the growth process. As the depth from the interface is increased, the Zn component decreases rapidly. While for the Mg atoms, their diffusion depth is more than 30 nm, as illustrated by the blue curve line. These results can be further confirmed by the depth profile of Mg-2p XPS spectra (Fig. 4(b)), which shows the existence of a weak peak of Mg-2p even at the depth of about 30 nm from the interface.

The PL spectrum at room temperature for the inclined film is shown in Fig. 5, which exhibits a blue shift of about 0.083 eV compared with the ZnO single crystal, as illustrated by the black arrows. This is probably due to the diffusion of Mg atoms into the ZnO film, thereby forming the ZnMgO alloy phase near the interface between ZnO and MgO, as discussed above. Interestingly, the room temperature PL spectra of this inclined film exhibits a very weak defect peaks at the region of the yellow light, as illustrated by the inset in Fig. 5, very similar to that of some high-quality or with multiple-fold-rotated ZnO films in previous reports [38,40–42]. We believe, this result on the one hand stems from this possibility that there exist a few defects in the ZnO grains. On the other hand, there really exist numerous boundary states among the grains, nonetheless, the luminescent spectra from the grain boundary states is different from that of the defects. Probably, the boundary states around the ZnO grain do not form some special energy level, like the defects. Therefore, the PL spectra from the multiple-fold-rotated ZnO films hardly exhibit the defect spectra peaks, as observed in this work and previous reports [38,40–42]. Moreover, the full width at

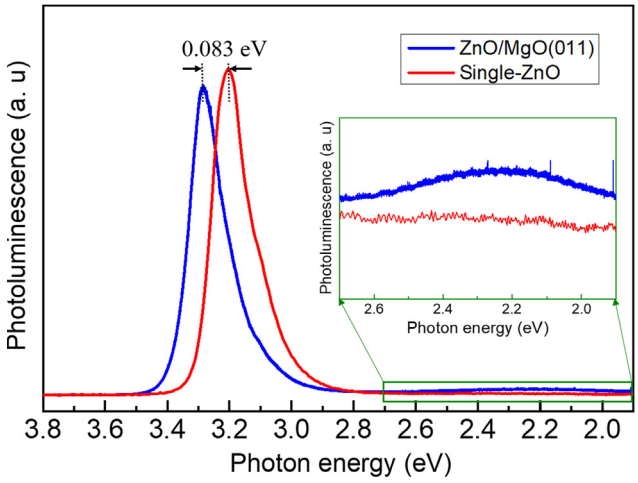

Fig. 5. Room temperature PL spectrum of the ZnO film (blue) and Single crystal (red), respectively, showing a blue shift of about 0.08 eV. The amplified image of the green rectangle shows a very weak but broad defect peak, as illustrated by the inset. (For interpretation of the references to colour in this figure legend, the reader is referred to the web version of this article.)

half maximum (FWHM) of the PL spectrum is just about 0.135 eV, almost identical to the single crystal (as shown by the red curve line in Fig. 5), which is close to the value (~0.117 eV) from the ZnO film of high quality film's in the previous reports [43]. This indicates that the inclined film possesses bulk-like optical property.

4. Conclusions

To sum up, a highly lattice-mismatched film through the coupling between ZnO and the MgO (0 1 1) substrate was prepared by the MBE method. The grown film is found to grow with a deviation of 31° from the c-axis and displays two-fold domains as well as the complex interface structures as follows: ± 1.66-tilited {$\bar{1}$ 0 1 3} (1 0 $\bar{1}$ 1)*[1 $\bar{2}$ 1 0]$_{ZnO\text{-}I}$//(0 1 1)[1 0 0][0 $\bar{1}$ 1]$_{MgO}$; ± 1.66-tilited {1 0 $\bar{1}$ 3}(1 0 $\bar{1}$ $\bar{1}$)*[1 $\bar{2}$ 1 0]$_{ZnO\text{-}II}$//(0 1 1)[1 0 0][0 $\bar{1}$ 1]$_{MgO}$. Moreover, there appear numerous atom diffusions at the interface, which leads to a blue shift of about 0.083 eV in the PL spectrum. However, the FWHM value is close to the bulk ZnO, suggesting high quality of optical property for the inclined ZnO film grown on the MgO (0 1 1) substrate.

Declaration of Competing Interest

The authors declared that there is no conflict of interest.

Acknowledgments

This work was financially support by the Chinese National Natural Science Foundation (Grant No. 11804050) and Fundamental Research Funds of Shandong University (Grant No. 11160079614062). The electron microscopy work at the Center for Functional Nanomaterials, BNL was supported by the U.S. Department of Energy, Office of Basic Energy Science (BES), Scientific User Facilities Division, under Contract No. DE-SC0012704.

Appendix A. Supplementary material

Supplementary data to this article can be found online at https://doi.org/10.1016/j.apsusc.2019.144781.

References

[1] C.-B. Eom, S. Trolier-McKinstry, Thin-film piezoelectric MEMS, MRS Bull. 37 (11) (2012) 1007–1017, https://doi.org/10.1557/mrs.2012.273.
[2] C. Dubourdieu, J. Bruley, T.M. Arruda, A. Posadas, J. Jordan-Sweet, M.M. Frank, E. Cartier, D.J. Frank, S.V. Kalinin, A.A. Demkov, V. Narayanan, Switching of ferroelectric polarization in epitaxial BaTiO(3) films on silicon without a conducting bottom electrode, Nat. Nanotechnol. 8 (10) (2013) 748–754, https://doi.org/10.1038/nnano.2013.192.
[3] X. An, F. Liu, Y.J. Jung, S. Kar, Tunable graphene-silicon heterojunctions for ultrasensitive photodetection, Nano Lett. 13 (3) (2013) 909–916, https://doi.org/10.1021/nl303682j.
[4] H. Bai, C. Li, G. Shi, Functional composite materials based on chemically converted graphene, Adv. Mater. 23 (9) (2011) 1089–1115, https://doi.org/10.1002/adma.201003753.
[5] S. Muthukumar, C.R. Gorla, N.W. Emanetoglu, S. Liang, Y. Lu, Control of morphology and orientation of ZnO thin films grown on SiO2/Si substrates, J. Cryst. Growth 225 (2–4) (2001) 197–201, https://doi.org/10.1016/s0022-0248(01)00874-0.
[6] J.H. Choi, H. Tabata, T. Kawai, Initial preferred growth in zinc oxide thin films on Si and amorphous substrates by a pulsed laser deposition, J. Cryst. Growth 226 (4) (2001) 493–500, https://doi.org/10.1016/s0022-0248(01)01388-4.
[7] P. Kung, A. Saxler, X. Zhang, D. Walker, T.C. Wang, I. Ferguson, M. Razeghi, High quality AIN and GaN epilayers grown on (00·1) sapphire, (100), and (111) silicon substrates, Appl. Phys. Lett. 66 (22) (1995) 2958–2960, https://doi.org/10.1063/1.114242.
[8] H. Ishikawa, G.Y. Zhao, N. Nakada, T. Egawa, T. Soga, T. Jimbo, M. Umeno, High-quality GaN on Si substrate using AlGaN/AlN intermediate layer, Phys. Status Solidi A-Appl. Res. 176 (1) (1999) 599–603, https://doi.org/10.1002/(sici)1521-396x(199911)176:1<599::Aid-pssa599>3.0.Co;2-f.
[9] R.C. Powell, N.E. Lee, Y.W. Kim, J.E. Greene, Heteroepitaxial wurtzite and zinc-blende structure GaN grown by reactive-ion molecular-beam epitaxy: growth kinetics, microstructure, and properties, J. Appl. Phys. 73 (1) (1993) 189–204, https://doi.org/10.1063/1.353882.
[10] S. Strite, An investigation of the properties of cubic GaN grown on GaAs by plasma-assisted molecular-beam epitaxy, J. Vac. Sci. Technol. B: Microelectron. Nanom. Struct. 9 (4) (1991), https://doi.org/10.1116/1.585381.
[11] L. Britnell, R.V. Gorbachev, A.K. Geim, L.A. Ponomarenko, A. Mishchenko, M.T. Greenaway, T.M. Fromhold, K.S. Novoselov, L. Eaves, Resonant tunnelling and negative differential conductance in graphene transistors, Nat. Commun. 4 (1) (2013), http://www.nature.com/articles/ncomms2817https://doi.org/10.1038/ncomms2817.
[12] D. Sinha, J.U. Lee, Ideal graphene/silicon Schottky junction diodes, Nano Lett. 14 (8) (2014) 4660–4664, https://doi.org/10.1021/nl501735k.
[13] E.Z. Shi, H.B. Li, L. Yang, L.H. Zhang, Z. Li, P.X. Li, Y.Y. Shang, S.T. Wu, X.M. Li, J.Q. Wei, K.L. Wang, H.W. Zhu, D.H. Wu, Y. Fang, A.Y. Cao, Colloidal antireflection coating improves graphene-silicon solar cells, Nano Lett. 13 (4) (2013) 1776–1781, https://doi.org/10.1021/nl400353f.
[14] Y. Song, X.M. Li, C. Mackin, X. Zhang, W.J. Fang, T. Palacios, H.W. Zhu, J. Kong, Role of interfacial oxide in high-efficiency graphene-silicon schottky barrier solar cells, Nano Lett. 15 (3) (2015) 2104–2110, https://doi.org/10.1021/nl505011f.
[15] L. Wang, J. Jie, Z. Shao, Q. Zhang, X. Zhang, Y. Wang, Z. Sun, S.-T. Lee, MoS2/Si heterojunction with vertically standing layered structure for ultrafast, high-detectivity, self-driven visible-near infrared photodetectors, Adv. Funct. Mater. 25 (19) (2015) 2910–2919, https://doi.org/10.1002/adfm.201500216.
[16] S.K. Dey, W. Cao, S. Bhaskar, J. Li, Highly textured Pb(Zr0.3Ti0.7)O3 thin films on GaN/sapphire by metalorganic chemical vapor deposition, J. Mater. Res. 21 (06) (2011) 1526–1531, https://doi.org/10.1557/jmr.2006.0184.
[17] Y.R. Li, J. Zhu, W.B. Luo, Study of the integrated growth of dielectric films on GaN semiconductor substrates, IEEE Trans. Ultrason. Ferroelectr. Freq. Control 57 (10) (2010) 2192–2197, https://doi.org/10.1109/tuffc.2010.1677.
[18] Bo Xiao, Xing Gu, Natalia Izyumskaya, Vitaliy Avrutin, Jinqiao Xie, Huiyong Liu, Hadis Morkoç, Structural and electrical properties of Pb(Zr,Ti)O3 grown on (0001) GaN using a double PbTiO3/PbO bridge layer, Appl. Phys. Lett. 91 (18) (2007) 182908 http://aip.scitation.org/doi/10.1063/1.2805220https://doi.org/10.1063/1.2805220.
[19] W.B. Luo, J. Zhu, H.Z. Zeng, X.W. Liao, H. Chen, W.L. Zhang, Y.R. Li, Effects of SrTiO3/TiO2 buffer layer on structural and electrical properties of BiFeO3 thin films grown on GaN (0002), J. Appl. Phys. 109 (10) (2011), https://doi.org/10.1063/1.3585836.
[20] F Scholz, Semipolar GaN grown on foreign substrates: a review, Semicond. Sci. Technol. 27 (2) (2012) 024002 http://stacks.iop.org/0268-1242/27/i=2/a=024002?key=crossref.78eeb9aae8392f2e8fdbf7a6bb66c634https://doi.org/10.1088/0268-1242/27/2/024002.
[21] R.M. Farrell, E.C. Young, F. Wu, S.P. DenBaars, J.S. Speck, Materials and growth issues for high-performance nonpolar and semipolar light-emitting devices, Semicond. Sci. Technol. 27 (2) (2012), https://doi.org/10.1088/0268-1242/27/2/024001.
[22] P. Waltereit, O. Brandt, A. Trampert, H.T. Grahn, J. Menniger, M. Ramsteiner, M. Reiche, K.H. Ploog, Nitride semiconductors free of electrostatic fields for efficient white light-emitting diodes, Nature 406 (6798) (2000) 865–868, https://doi.org/10.1038/35022529.
[23] G. Li, H. Yang, Epitaxial growth of high quality nonpolar InN films on LiGaO2 substrates, Cryst. Growth Des. 11 (3) (2011) 664–667, https://doi.org/10.1021/cg1007473.
[24] G.Q. Li, S.J. Shih, Epitaxial Growth and Characterisation of Nonpolar M-Plane GaN on LaAlO(3) Substrate, IEEE, New York, 2010 pp. 1205–1205.
[25] U. Ozgur, Y.I. Alivov, C. Liu, A. Teke, M.A. Reshchikov, S. Dogan, V. Avrutin, S.J. Cho, H.A. Morkoc, comprehensive review of ZnO materials and devices, J. Appl. Phys. 98 (4) (2005) 103, https://doi.org/10.1063/1.1992666.
[26] Z.L. Wang, J.H. Song, Piezoelectric nanogenerators based on zinc oxide nanowire arrays, Science 312 (5771) (2006) 242–246, https://doi.org/10.1126/science.1124005.
[27] J.-H. Shen, S.-W. Yeh, H.-L. Huang, D. Gan, N.-J. Ho, Low-temperature preparation of undoped ZnO films with high transparency and conductivity by ion beam deposition, J. Electron. Mater. 39 (5) (2010) 612–618, https://doi.org/10.1007/s11664-010-1130-7.
[28] C.H. Jia, Y.H. Chen, X.L. Liu, S.Y. Yang, W.F. Zhang, Z.G. Wang, Control of epitaxial relationships of ZnO/SrTiO3 heterointerfaces by etching the substrate surface, Nanosc. Res. Lett. 8 (2013) 8, https://doi.org/10.1186/1556-276x-8-23.
[29] E. Cagin, J. Yang, W. Wang, J.D. Phillips, S.K. Hong, J.W. Lee, J.Y. Lee, Growth and structural properties of m-plane ZnO on MgO (001) by molecular beam epitaxy, Appl. Phys. Lett. 92 (23) (2008), https://doi.org/10.1063/1.2940305.
[30] Hua Zhou, Lijun Wu, Hui-Qiong Wang, Jin-Cheng Zheng, Lihua Zhang, Kim Kisslinger, Yaping Li, Zhiqiang Wang, Hao Cheng, Shanming Ke, Yu Li, Junyong Kang, Yimei Zhu, Interfaces between hexagonal and cubic oxides and their structure alternatives, Nat. Commun. 8 (1) (2017), http://www.nature.com/articles/s41467-017-01655-5https://doi.org/10.1038/s41467-017-01655-5.
[31] A. Bera, H. Peng, J. Lourembam, Y. Shen, X.W. Sun, T. Wu, A versatile light-switchable nanorod memory: wurtzite ZnO on perovskite $SrTiO_3$, Adv. Funct. Mater. 23 (39) (2013) 4977–4984, https://doi.org/10.1002/adfm.201300509.
[32] S.J. Henley, M.N.R. Ashfold, D. Cherns, The oriented growth of ZnO films on NaCl substrates by pulsed laser ablation, Thin Solid Films 422 (2002) 69–72.
[33] J.H. Choi, H. Tabata, Tomoji Kawai, Initial preferred growth in zinc oxide thin films on Si and amorphous substrates by a pulsed laser deposition, J. Crys. Growth 226 (2001) 493–500.
[34] C.T. Campbell, J. Sauer, Introduction: surface chemistry of oxides, Chem. Rev. 113 (6) (2013) 3859–3862, https://doi.org/10.1021/cr4002337.
[35] M. Sterrer, T. Risse, P.U. Martinez, L. Giordano, M. Heyde, H.P. Rust, G. Pacchioni, H.J. Freund, Control of the charge state of metal atoms on thin MgO films, Phys. Rev. Lett. 98 (9) (2007) 096107, https://doi.org/10.1103/PhysRevLett.98.096107.
[36] X. Jiang, R. Wang, R.M. Shelby, R.M. Macfarlane, S.R. Bank, J.S. Harris, S.S. Parkin, Highly spin-polarized room-temperature tunnel injector for semiconductor spintronics using MgO(100), Phys. Rev. Lett. 94 (5) (2005) 056601, https://doi.org/10.1103/PhysRevLett.94.056601.
[37] R. Suzuki, A. Kawaharazuka, Y. Horikoshi, MBE growth of GaN on MgO substrate, J. Cryst. Growth 301–302 (2007) 478–481, https://doi.org/10.1016/j.jcrysgro.2006.11.095.
[38] H. Zhou, H.Q. Wang, Y. Li, K. Li, J. Kang, J.C. Zheng, Z. Jiang, Y. Huang, L. Wu, L. Zhang, K. Kisslinger, Y. Zhu, Evolution of wurtzite ZnO films on Cubic MgO (001) substrates: a structural, optical, and electronic investigation of the misfit structures, ACS Appl. Mater. Interfaces 6 (16) (2014) 13823–13832, https://doi.org/10.1021/am503256p.
[39] Grégory Geneste, Joseph Morillo, Fabio Finocchi, Adsorption and diffusion of Mg, O, and O2 on the MgO(001) flat surface, J. Chem. Phys. 122 (17) (2005) 174707 http://aip.scitation.org/doi/10.1063/1.1886734https://doi.org/10.1063/1.1886734.
[40] Y.F. Chen, S.K. Hong, H.J. Ko, M. Nakajima, T. Yao, Y. Segawa, Plasma-assisted molecular-beam epitaxy of ZnO epilayers on atomically flat $MgAl_2O_4$(111) substrates, Appl. Phys. Lett. 76 (2000) 245–247.
[41] H.F. Liu, S.J. Chu, G.X. Hu, H. Gong, N. Xiang, Effects of substrate on the structure and orientation of ZnO thin film grown by rf-magnetron sputtering, J. Appl. Phys. 102 (2007) 083529.
[42] J.H. Shen, S.W. Yeh, S.W. Mao, H.L. Huang, Y.S. Huang, D. Gan, Visible photoluminescense of the (110), (101) and (0001) surfaces of ZnO nanofilms, Mater. Lett. 65 (2011) 3333–3335.
[43] Y. Chen, D.M. Bagnall, H.-J. Koh, K.-T. Park, K. Hiraga, Z. Zhu, T. Yao, Plasma assisted molecular beam epitaxy of ZnO on c -plane sapphire: growth and characterization, J. Appl. Phys. 84 (7) (1998) 3912–3918, https://doi.org/10.1063/1.368595.